An Imperceptible Plastic Electronic Wrap

Michael Drack, Ingrid Graz, Tsuyoshi Sekitani, Takao Someya, Martin Kaltenbrunner, and Siegfried Bauer*

Electronics is evolving from accompanying appliances to an imperceptible form, wearable as glasses, textiles[1] and medical prostheses,[2] directly adherent to the skin[3] or inner organs like the heart[4] and the brain,[5] establishing a seamless link between living beings and electronic devices. Biodegradable,[6,7] transient[8] and edible[9–11] forms of electronics provide further opportunities for applications in healthcare, food, and environmental quality monitoring.[12–14]

Flexibility, compliance, weight, and softness will turn out to be key metrics in next-generation smart electronic appliances. Ultraflexible and lightweight solar cells,[15] organic light-emitting diode displays[16] and active-matrix sensor arrays[17] are first demonstrations toward imperceptible devices that camouflage their presence. However, success in consumer markets requires extended durability and routes to employ readily existing materials, components, and production techniques. Here, we show highly reliable, flexible and stretchable metallic and transparent organic conductors with near-bulk-metal electrical resistivities (32.6 nΩ m for Al, 20.1 nΩ m for Ag, 17.1 nΩ m for Cu, 25.5 nΩ m for Au) that enable temperature mapping on complex 3D objects like integrated circuits on printed circuit boards, food packages, and on human skin.[18] In their stretchable form, our metal films withstand strains up to 275%; Au and industrially relevant[19] Cu metal films endure more than 1000 cycles of stretching to 50% without appreciable decrease in conductivity. The imperceptible electronic foil technology platform offers new avenues for the design of complex, stretchable electronic devices based on the hybrid rigid-island–stretchable-interconnect concept.[20,21] We show this with highly stretchable RGB and white LED strips that can be twisted and stretched to over 140% and 2D arrays biaxially stretched to 2.5 times their initial area repeatedly without failure.

M. Drack, Dr. I. Graz, Dr. M. Kaltenbrunner, Prof. S. Bauer
Department of Soft Matter Physics
Johannes Kepler University
Altenbergerstrasse 69, 4040 Linz, Austria
E-mail: Michael.Drack@jku.at
Prof. T. Sekitani, Prof. T. Someya
Electrical and Electronic Engineering and Information Systems
The University of Tokyo
7–3–1 Hongo, Bunkyo-ku, Tokyo 113–8656, Japan
Prof. T. Sekitani, Prof. T. Someya
Exploratory Research for Advanced Technology (ERATO)
Japan Science and Technology Agency (JST)
2–11–16, Yayoi, Bunkyo-ku, Tokyo 113–0032, Japan

DOI: 10.1002/adma.201403093

The ultrathin foil is temporarily adhered to a reusable support (**Figure 1**a). This allows all subsequent processing steps to be scalable by adopting a roll-to-roll fabrication scheme. Ultrathin poly(ethylene terephthalate) (PET) and poly(ethylene naphthalate) (PEN) foils with thickness in the micrometer range are commercially available at low cost in rolls for foil capacitors[22,23] (Figure 1b). After fabrication, the foil is simply peeled from the temporary support. Weighing only 3 g/m^2, our ultrathin electronic foils float on soap films (Figure 1c, and Video S1 in the Supporting Information), and intimately conform to complex 3D objects like printed circuit boards (Figure 1d), creating a form of electronic plastic kitchen wrap. A one-step transfer process of the wrap to a soft material, like a pre-stretched elastomer, results in a functional hybrid that paves the way for high-performance rigid-island–stretchable-interconnect electronic systems. Strips with surface-mounted device (SMD) LEDs mounted on such a composite of elastomer and ultrathin foil survive twisting and stretching without having their functionality impaired (Figure 1e).

We first demonstrate the use of imperceptible electronic films as sensitive and compliant temperature sensors on printed circuit boards (**Figure 2**a), food items (Figure 2b) and human skin (Figure S1, Supporting Information). 100-nm-thick films of gold, copper, aluminum, and silver are thermally evaporated onto flat 1.4-µm-thick PET foils. The extremely small bending radius allows the sensor foil to wrap tightly around the electronic components of the printed circuit board and to monitor the exponential rise and the saturation of the temperature during device operation (Figure 2a). Placed on a package of frozen fish, the thin-film sensors measure the complete defrosting period of the fish (more than 15 h) with remarkable accuracy (Figure 2b). A thin water film forms on the sensor foil during melting, which is reflected in a small increase of noise during the temperature recording. These harsh conditions, however, do not impair the reliability of the measurement. Precise spatio-temporal temperature mapping on the human skin is an important tool for diagnostics.[18] Attached to the nose, our sensors follow on-skin temperature changes induced by drinking a cup of hot tea and subsequently a glass of cold water (Figure S1, Supporting Information). Our approach does not require microstructuring techniques and is a low-cost solution for accurate temperature recording where ultrahigh spatial resolution is not needed. Details of the calibration and the temperature coefficients of the resistivity of the thin metal films used are given in Figure S2 in the Supporting Information. The thin-film-sensor temperature recordings on the integrated electronic circuit, on the food package, and on-skin show remarkable agreement with infrared camera recordings (Figure 2a,b and Figure S1 in the Supporting Information) and fortify the sensor's potential as a low-cost solution for consumer electronics survey, food quality monitoring, and disposable patches in healthcare.

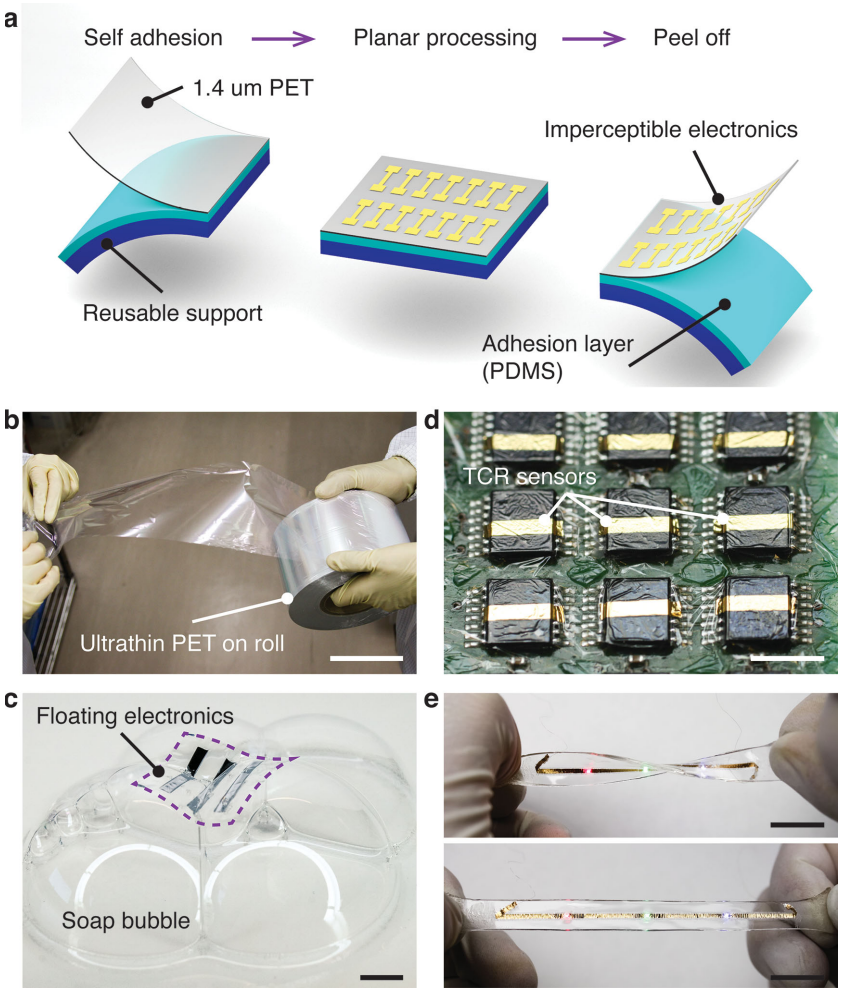

Figure 1. a) Scheme for the preparation of imperceptible electronic conductors: the 1.4 μm PET foil is mounted on a reusable support with a PDMS adhesion layer. After planar processing of the electrodes and peeling, the skin-spired electronic device is ready to use. b) Ultrathin capacitor foils on rolls form the technology platform for large-area sensor and electronic circuits. Scale bar: 10 cm. c) Photograph of the ultrathin electronic film floating on a soap bubble. Scale bar: 5 mm. d) TCR sensor array conformably coating a PCB board for temperature monitoring. Scale bar: 5 mm. e) Hybrid rigid RGB LED islands connected with stretchable conductors, formed by transferring the electrode stripes onto a pre-stretched elastomer, survive twisting and stretching. Scale bar: 1 cm.

Blurring the boundaries between the digital and biological world further requires electronic devices to be soft and stretchable. Evolving from elastic conductors[24] based on microcracks,[25,26] serpentines,[27,28] out-of-plane folds,[29] conducting composites,[30,31] nanowires,[32,33] carbon-nanotube networks,[34] crumpled graphene,[35] and ionic hydrogels,[36] stretchable electronics is rapidly developing into a mainstream future technology.[21,37] However, it remains challenging to achieve conductors with high stretchability, metallic and strain-independent conductivity, and high cyclic endurance simultaneously. Imperceptible electronics, with its extreme flexibility, offers an elegant, potentially low-cost route to stretchable interconnects with strain-independent, near-bulk-metal conductivities for ultracompliant devices. A facile one-step transfer of the imperceptible foil onto a pre-stretched elastomer forms highly stretchable electrical conductors (**Figure 3**a). The elastomeric substrate can be chosen to match device-specific requirements, 3M VHB tapes enable large strains exceeding 200%. Out-of-plane wrinkling of the foil when the elastomer is relaxed permits repeatable stretchability up to 275% tensile strain (Figure 3b). The image sequence displays the stretching of a copper metal electrode from the fully wrinkled to the flat state. Here, the pre-stretch of the elastomer and the packing density of the fully compressed folds define the maximum strain. Localized high-aspect-ratio ridge wrinkles form, which enable the high stretchability of the stiff metal-film–polymer-support structure that is resting on the soft elastomer.[38] A magnified view of this wrinkle morphology shows wavelengths between 100–250 μm and amplitudes up to 100 μm. (Figure 3c). The buckled morphology of the imperceptible electronic foil results in a strain-independent conductivity of the stretchable copper electrode (Figure 3d). The normalized electric resistance is perfectly reversible for almost 300% strain. Such metallic interconnects are ideal building blocks for a versatile stretchable electronic platform where rigid active components are placed on strain-insulated islands. We demonstrate this concept with highly stretchable light strips, where SMD LEDs rest on 50-μm-thick polyimide reinforcements[39,40] that are embedded in a VHB tape sandwich to locally stiffen the elastomeric substrate (Figure 3e). White-light-emitting LEDs endure twisting and stretching up to 240% with unaltered performance (Video S2 and Figure S3 and S4, Supporting Information), a multicolored strip with red, green, and blue SMD LEDs is stretched to 140% and twisted by 720° simultaneously (Figure 3f–h). A more-sophisticated 2D network of LEDs that is biaxially stretched to an area expansion rate of 2.5 without impairing the function (Figure 3i,j, and Video S3 and Figure S5 in the Supporting Information) outlines the potential of this complementary approach for soft assemblies of high-performance, off-the-shelf electronic components.[41,42]

Cyclic endurance is critically important for the transition from laboratory demonstrators to real-world products. Identifying and understanding failure mechanism will help in assessing optimal materials and guide device designs. We investigated the fatigue characteristics of Al-, Ag-, Au-, and Cu-based imperceptible conductors cyclically stretched to 50%. While undergoing a stretching cycle, multiple folds with radii of curvature as small as 5 μm form in the imperceptible foil. In this manner, the endurance toward bending and folding is assessed as well. Two exemplary stretch cycles of an Ag sample are shown in Video S4 in the Supporting Information; details

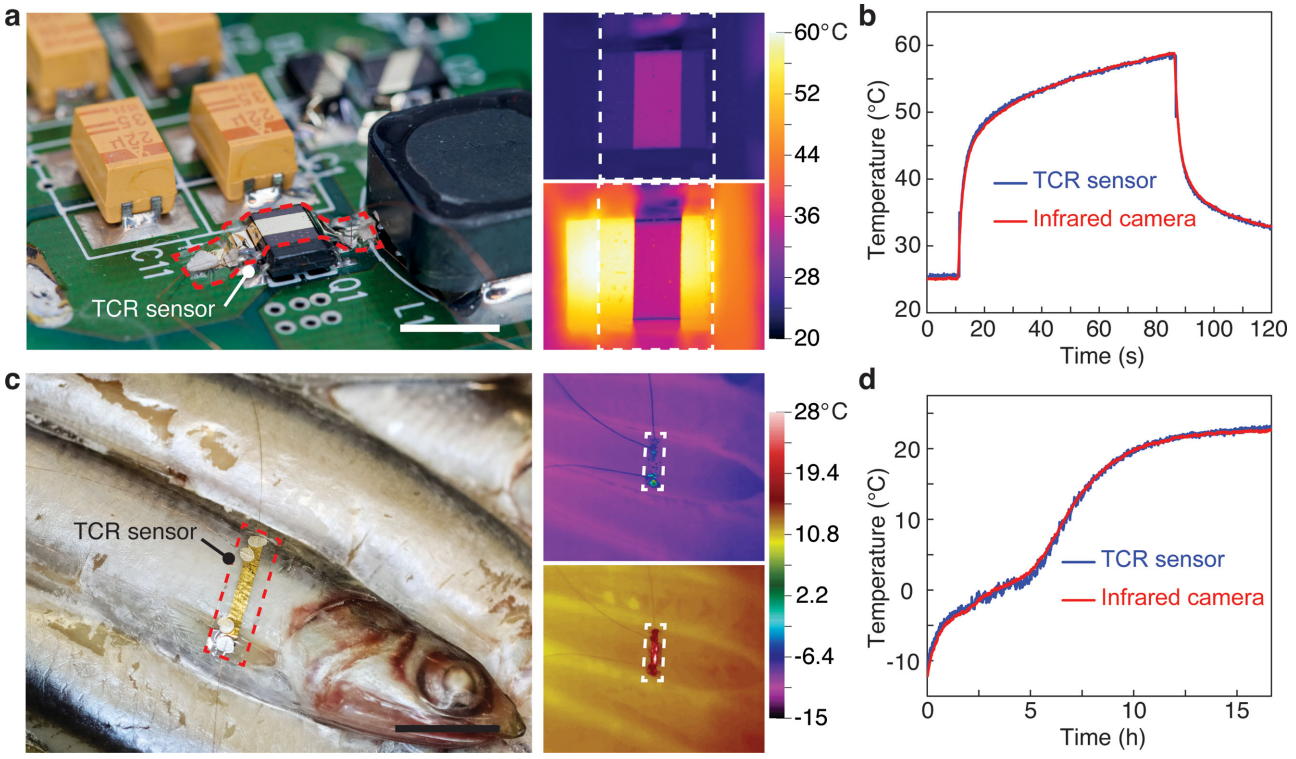

Figure 2. Temperature monitoring on: a,b) printed circuit boards and c,d) on food items. a) TCR circuit mounted conformably on a PCB board (left) and IR camera recordings of the circuit in OFF (top right) and ON (bottom right) state. Scale bar: 5 mm. b) Comparison of temperature recording between the TCR sensor and the IR camera. c) Packaged frozen fish equipped with a TCR sensor (left) together with IR camera recordings in the frozen (top right) and thawed state (bottom right). Scale bar: 1 cm. d) Temperature profile during defrosting (right).

of the test setup are found in the Experimental Section and Supporting Information. An elastomeric double layer with poly(dimethylsiloxane) (PDMS) underneath the VHB tape is used to enhance the reliability of the stretchable support[43] and to suppress viscous drifts of the acrylic VHB elastomer during long-term testing. A distinctly different evolution of the electrical resistance is found for the investigated metals as the cycle number increases up to 1000 cycles (**Figure 4**a). Stretchable aluminum conductors start to show an increase in resistance after roughly 20 cycles and typically fail after 400 cycles. Silver-based conductors show a less pronounced deterioration after 200 cycles; they roughly double their resistance after 1000 cycles but do not fail catastrophically. Gold and copper thin films are highly reliable and show no signs of fatigue even after 1000 stretch cycles. A detailed analysis of the first stretch cycle shows the expected strain-independence of the resistance for all four metals (Figure 4b). For Al, later cycles reveal a steady increase in resistance that remains independent of strain. In contrast, Ag shows a distinct stretch-dependent resistance after 1000 fatigue cycles, with 20% resistance increase at 0% strain and nearly double the initial value at maximum strain. Again, Au and Cu show no signs of degradation with nearly overlapping traces recorded for the first and last cycle. We explain these observations and identify failure mechanisms by scanning electron microscopy (SEM) imaging of the fatigued samples. Aluminum samples exhibit pronounced cracking and delamination in the valleys, but not on the hills of the folds perpendicular to the stretching direction (Figure 4c, and Figure S6 in the Supporting Information). Once opened, cracks immediately form a natural oxide layer which results in a steady, strain-independent increase of resistance. Silver electrodes show cracks at both hills and valleys of the folds with a less pronounced delamination (Figure 4d, and Figure S7 in the Supporting Information). Here, cracking at the hills results in a steady increase of resistance even at 0% strain, whereas the strain-induced opening and closing of the cracks at the valleys causes the pronounced strain dependence observed in the electrical resistance (Figure 4b). The SEM images of both gold and copper films show neither cracks nor delamination even after 1000 stretch cycles (Figure 4e,f). A special case was observed for some of the Au-based stretchable conductors, where the 1.5-μm-thick metallized PET forms deep folds upon the first compression of the VHB-PDMS sandwich. In this case, extreme compressive strains at the bottom of those deep folds form long cracks even for Au. A detailed analysis of the mechanisms for this case is given in Figure S8 in the Supporting Information. Our observations corroborate the importance of both the choice of the metallic conductor and a suitable elastomeric support. Among the tested metals, we find that Cu is the most reliable with no signs of fatigue after 1000 test cycles to 50% strain. Future research can be directed to optimize and investigate structures with the conductive components placed in the neutral strain position, and testing other metals or alloys, adhesion layers and deposition techniques.

Metals are excellent conductors, but they display a rather strong mechanical mismatch to polymer substrates. Polymer

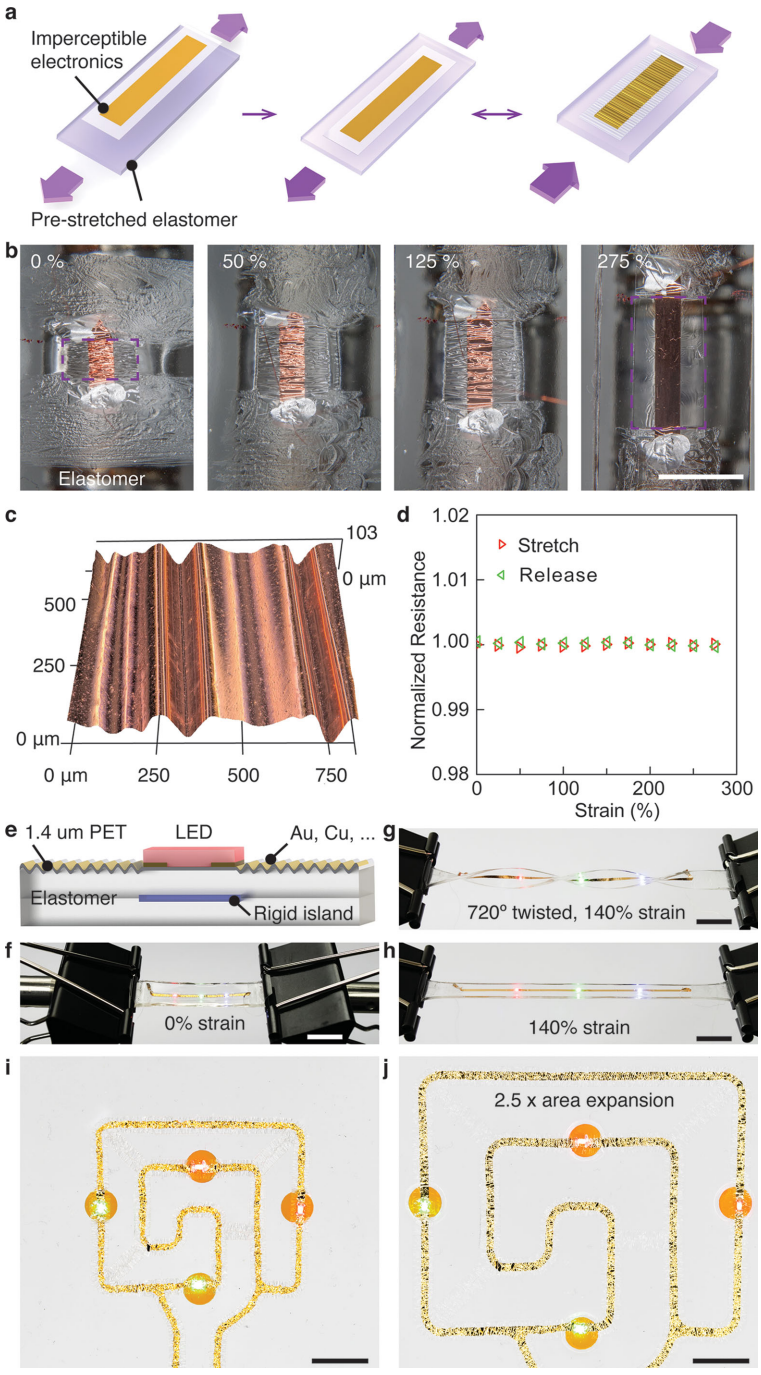

Figure 3. a) Scheme for the preparation of highly reliable stretchable conductors: The electronic foil is transferred onto a pre-stretched elastomer (left, middle) forming out-of plane wrinkles upon release (right). b) The image sequence displays a highly wrinkled stretchable copper conductor in the relaxed state (far left) and its subsequently flattening out when stretched to 50% (left) and 125% (right) strain. At the maximum strain of 275% the electrode is smooth (far right). Scale bar: 5 mm. c) 2D-profilometric microscopic image of the surface topography of a copper electrode with 50% pre-stretch. d) Normalized resistance of the copper electrode stretched to 275% strain remains constant. e) Scheme of the hybrid rigid-island approach: stiff polyimide (PI) islands are embedded between two layers of acrylic elastomer. The top elastomer layer carries the stretchable interconnects and the LEDs. LEDs are located above the rigid islands. f–h) Photographs of the hybrid LED strip during stretching from 0% (f) to 140% strain (h) and additional twisting by 720° (g). Scale bars: 15 mm. i,j) Photographs of the relaxed (i) and biaxially stretched (j) LED array with an areal expansion factor of 2.5. Scale bars: 5 mm

conductors on the other hand, have an elastic modulus comparable to that of the thin-film PET substrate, making them interesting for stretchable and elastic conductors. Poly(3,4-ethylenedioxythiophene) :poly(styrenesulphonate) (PEDOT:PSS) is an organic conductor with a specific resistance of 11.88 µΩ m for the Clevios PH1000 formulation. In the stretched state the conducting film is transparent, while in the wrinkled state the film becomes translucent due to light scattering at the wrinkled surface (**Figure 5**a). The initial resistance of 330 Ω for the 120-nm-thick PEDOT:PSS film is about 100× higher than that of our metallic conductors. Here, the dimensions of the test sample are identical to those with metal electrodes, but the conductive ink layer is prepared by spin-coating and covers the whole width of the PET strip, making the conductor twice as wide. Fatigue experiments show no change in the resistance for the first 100 cycles, a slight increase to 365 Ω after 1000 cycles, and a still fully functional electrode after 10 000 cycles with a resistance increase up to 430 Ω (Figure 5b). The resistance profile shows no strain dependence when stretched up to 50%, similar to the behavior of Al films. While the resistance slightly increases by 30% over the course of 10 000 cycles, we have found no indication of the fracture of the PEDOT:PSS. The resistance increase may be attributed to the operation in ambient air and the potential water uptake during fatigue.[44] Such highly reliable transparent electrodes form the basis of highly stretchable optoelectronic devices.[15,16]

In summary, we have investigated different metals as stretchable conductors for imperceptible electronics. Au, Cu, and PEDOT:PSS were found to be highly reliable, withstanding 1000 stretch cycles for the metals, and 10 000 for the polymer conductor without failure. Al and Ag films show cracks in the hills or in the valleys when repeatedly stretched and relaxed, but operation in neutral plane configurations may prevent these cracks. We developed an imperceptible electronic conductor platform that forms a versatile route for sophisticated stretchable electronic devices based on the rigid-island–stretchable-interconnect approach.

Experimental Section

Substrate Preparation: To simplify handling, the 1.4-µm-thick PET foil was temporarily attached to a reusable support substrate foil (125-µm-thick PET covered with a thin PDMS adhesion layer). This allows for all-planar device fabrication and the subsequent defect-free peeling or transfer of the completed device to a pre-stretched elastomer (see Figure 3a).

Thin-Film Conductor Preparation: Metal conductors on the ultrathin PET foil utilized 3 nm Cr as an adhesion layer underneath the 100-nm-thick metal film, prepared by thermal evaporation through a shadow mask (12 mm × 1.5 mm formed one conductor stripe). Silver, gold, and copper were

ADVANCED MATERIALS
www.advmat.de

www.MaterialsViews.com

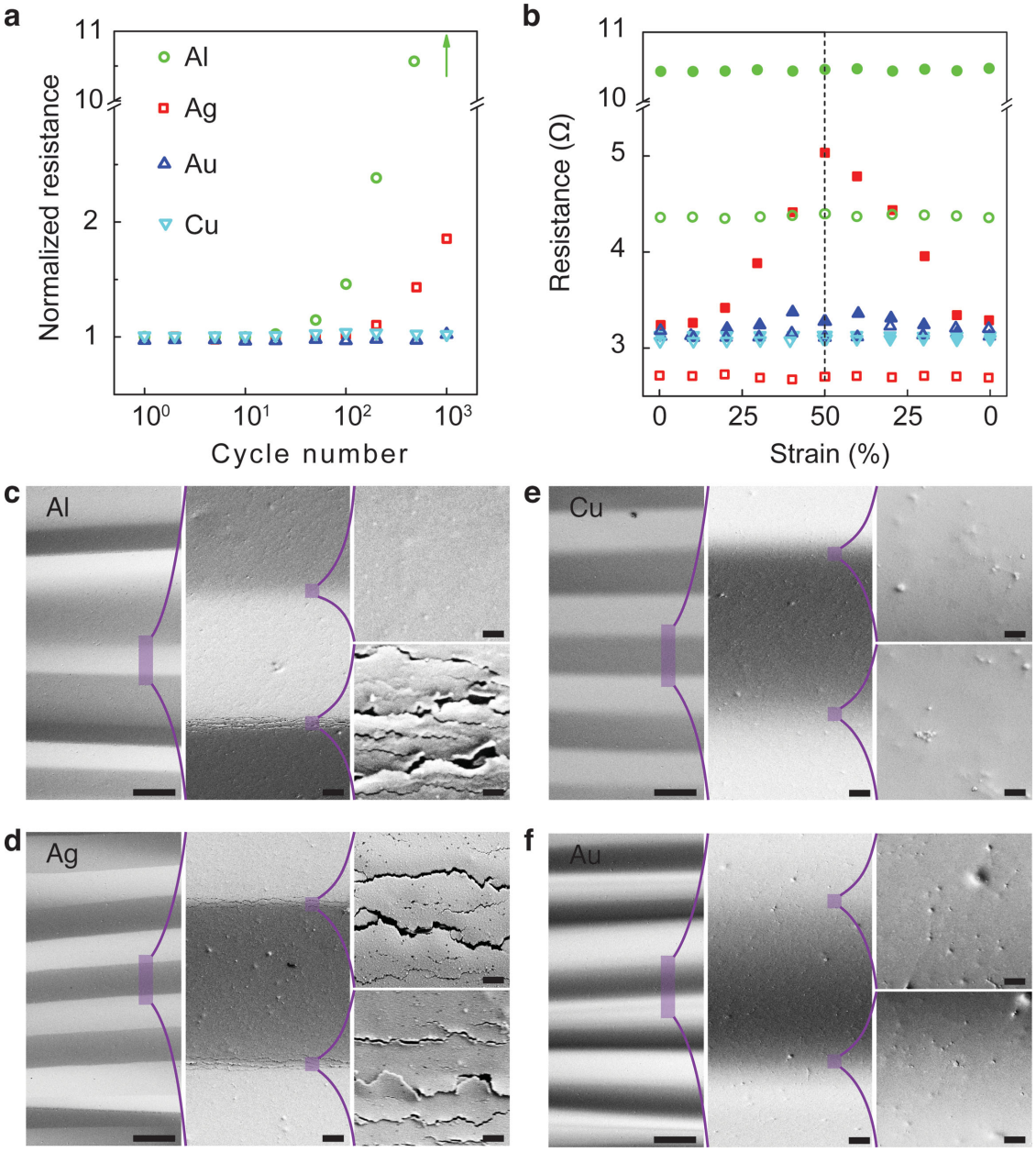

Figure 4. Fatigue and reliability of the stretchable conductors: a) normalized resistance versus cycle number for stretchable copper (cyan upside-down triangles), gold (blue triangles), aluminum (green circle) and silver (red square) samples up to 1000 cycles and 50% maximum strain. The resistance is unaffected for copper and gold, whereas it increases for aluminum and silver after 20 and 200 cycles, respectively. b) Resistance of different metals versus strain for the initial (empty symbols) and final (1000 for Ag, Au and Cu, 400 for Al) stretching-releasing cycle (filled symbols) up to a maximum of 50% strain. All the metals show a stretch independent resistance for the first cycle. At cycle 1000, only silver shows a strain-dependent resistance, increasing with stretching and decreasing upon release. For aluminum, the resistance remains constant during a single cycle, and electrodes typically fail after 400 cycles. c–f) SEM images at 50% strain for fatigued aluminum (c), silver (d), copper (e), and gold (f) conductors. The image sequence for each metal displays an overview (left), a single fold (middle) and a close-up at the hill and valley (right top and bottom). Aluminum cracks in the valleys with severe delamination, silver exhibits cracks in hills and valleys, whereas copper and gold remain crack free. Scale bars: 100 μm, 10 μm, 1 μm respectively. The variation of shadows cast by hills and valleys stems from the mounting in the SEM without impairing the results.

evaporated with a rate of 0.2 nm/s. Aluminum films were prepared by flash evaporation. Transparent electrodes with a thickness of 120 nm and with 130 Ω per square were prepared by spin-coating PEDOT:PSS (PH1000, Clevios) with 5% dimethylsulfoxide, mixed with 0.5% Zonyl FS-300 fluorosurfactant (Fluka) to promote wetting on the hydrophobic PET at 1000 rpm for 60 s, followed by 2000 rpm for 60 s. The samples were dried on a hotplate for 10 min at 120 °C.

Hybrid Rigid-Island LED Strips: Polyimide rigid islands (2 mm × 2 mm area) with a pitch of 9 mm were sandwiched between 2 VHB 4910 elastomer tapes. The elastomer stack was pre-stretched (between 140 and 240%) and the PET foil supporting the gold conductors was transferred. White and RGB SMD LEDs (0402, Osram) were pinned to the VHB above the rigid-island areas with Elastosil (Wacker). Electrical contacts between stretchable conductors and LEDs were ensured by

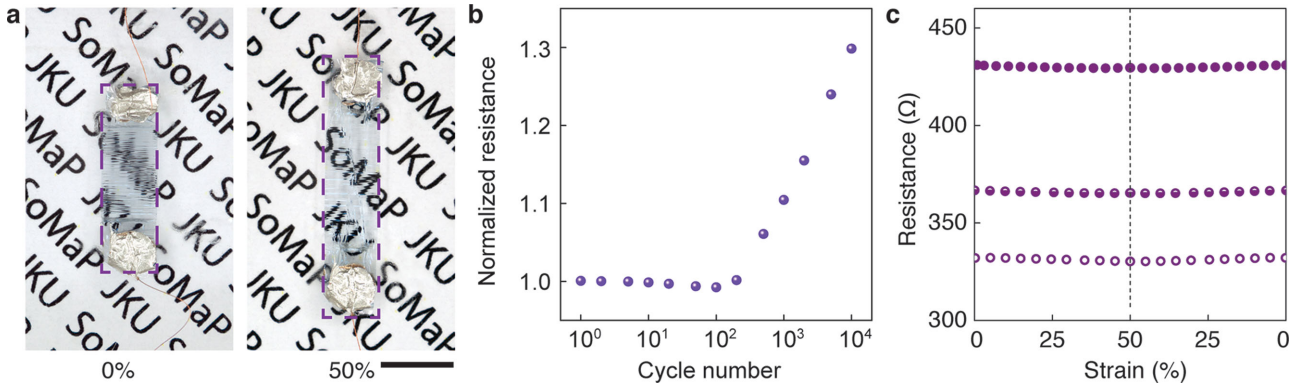

Figure 5. Transparent and translucent stretchable organic conductor. a) Photographs of a translucent wrinkled and transparent flat PEDOT:PSS film. Scale bar: 2 mm. b) Normalized resistance versus cycle number for PEDOT:PSS. The resistance starts to increase after 200 cycles with only 30% rise after 10 000 cycles. c) Resistance versus strain for the initial (empty symbols), the 1000th (half-filled) and 10 000th cycle (filled symbols) up to 50% strain.

means of silver dag. The LED circuit was driven with a constant current of 5 mA by a Keithley 2612 Sourcemeter.

Stretchable 2D-LED Arrays: Circular polyimide islands (3 mm diameter) were embedded between 2 VHB 4910 sheets. A Au conductor array layout was thermally evaporated on the PET foil. Excess substrate material was removed with a laser cutter (Trotec Speedy 300) before transferring onto the 100% biaxially pre-stretched VHB-rigid island sandwich. SMD LEDs were placed and contacted with conductive epoxy (Circuitworks CW2400). The circuit was driven with a constant current of 10 mA by a Keithley 2612 Sourcemeter.

Thermal Sensors: The PET foil was removed from the support and directly transferred onto integrated circuits or on frozen food. For thermal measurements on the skin, the sensor was adhered with band-aid spray (Hansaplast). All the resistance measurements were conducted in a 4-wire configuration with a Keithley 2000 Multimeter. An FLIR A325sc system camera was used for thermal imaging.

Cyclic Fatigue Testing of Stretchable Electrodes: The PET foil supporting the electrode was peeled from the carrier substrate and transferred onto a pre-stretched elastomer sandwich consisting of a 1 mm layer of VHB 4910 atop a 1-mm-thick PDMS layer (Sylgard 184, Dow Corning, 10:1 mixing ratio). This engineered double layer drastically reduces viscous drift of the VHB tape during cyclic stretching. The electromechanical characterization was performed with a tensometer. Samples were mounted on a home-built computer-controlled uniaxial stretcher driven by a stepper motor. The resistance change was measured between two-point probes using a Keithley 2000 multimeter in the ohmmeter configuration. Silver dag ensured electrical contact between the stretchable electrode and the copper wires connected up to the ohmmeter. The samples were stretched up to 50% with a strain rate of 0.94%/s while continuously recording the resistance. All the metal conductors where cycled up to 1000 times (Ag, Au, and Cu) or until failure (Al, ca. 400 times), the conducting polymer PEDOT:PSS was fatigued up to 10 000 cycles.

Supporting Information

Supporting Information is available from the Wiley Online Library or from the author.

Acknowledgements

This work partially supported by the Austrian Science Fund (FWFP22912-N20), by COST in the framework of ESNAM (MP1003), and by the ERC Advanced Research Grant "Soft Map". The work in Tokyo was supported by the JST Someya Bio-Harmonized ERATO grant. The authors thank Klaus Haselgrübler and Günther Hesser for their help with the SEM images, Wolfgang Hilber for Cu sample preparation, and Stefan Schausberger for help with experimental setups.

Received: July 10, 2014
Revised: August 26, 2014
Published online: October 20, 2014

[1] K. Cherenack, L. van Pieterson, *J. Appl. Phys.* **2012**, *112*, 091301.
[2] T. Ware, D. Simon, R. L. Rennaker, W. Voit, *Polym. Rev.* **2013**, *53*, 108.
[3] D.-H. Kim, N. Lu, R. Ma, Y.-S. Kim, R.-H. Kim, S. Wang, J. Wu, S. M. Won, H. Tao, A. Islam, K. J. Yu, T. Kim, R. Chowdhury, M. Ying, L. Xu, M. Li, H.-J. Chung, H. Keum, M. McCormick, P. Liu, Y.-W. Zhang, F. G. Omenetto, Y. Huang, T. Coleman, J. A. Rogers, *Science* **2011**, *333*, 838.
[4] L. Xu, S. R. Gutbrod, A. P. Bonifas, Y. Su, M. S. Sulkin, N. Lu, H.-J. Chung, K.-I. Jang, Z. Liu, M. Ying, C. Lu, R. C. Webb, J.-S. Kim, J. I. Laughner, H. Cheng, Y. Liu, A. Ameen, J.-W. Jeong, G.-T. Kim, Y. Huang, I. R. Efimov, J. A. Rogers, *Nat. Commun.* **2014**, *5*, 3329.
[5] J. Viventi, D.-H. Kim, L. Vigeland, E. S. Frechette, J. A. Blanco, Y.-S. Kim, A. E. Avrin, V. R. Tiruvadi, S.-W. Hwang, A. C. Vanleer, D. F. Wulsin, K. Davis, C. E. Gelber, L. Palmer, J. Van der Spiegel, J. Wu, J. Xiao, Y. Huang, D. Contreras, J. A. Rogers, B. Litt, *Nat. Neurosci.* **2011**, *14*, 1599.
[6] D.-H. Kim, J. Viventi, J. J. Amsden, J. Xiao, L. Vigeland, Y.-S. Kim, J. A. Blanco, B. Panilaitis, E. S. Frechette, D. Contreras, D. L. Kaplan, F. G. Omenetto, Y. Huang, K.-C. Hwang, M. R. Zakin, B. Litt, J. A. Rogers, *Nat. Mater.* **2010**, *9*, 511.
[7] C. J. Bettinger, Z. Bao, *Adv. Mater.* **2010**, *22*, 651.
[8] S.-W. Hwang, D.-H. Kim, H. Tao, T. Kim, S. Kim, K. J. Yu, B. Panilaitis, J.-W. Jeong, J.-K. Song, F. G. Omenetto, J. A. Rogers, *Adv. Funct. Mater.* **2013**, *23*, 4087.
[9] M. Irimia-Vladu, P. A. Troshin, M. Reisinger, L. Shmygleva, Y. Kanbur, G. Schwabegger, M. Bodea, R. Schwödiauer, A. Mumyatov, J. W. Fergus, V. F. Razumov, H. Sitter, N. S. Sariciftci, S. Bauer, *Adv. Funct. Mater.* **2010**, *20*, 4069.
[10] H. Tao, M. A. Brenckle, M. Yang, J. Zhang, M. Liu, S. M. Siebert, R. D. Averitt, M. S. Mannoor, M. C. McAlpine, J. A. Rogers, D. L. Kaplan, F. G. Omenetto, *Adv. Mater.* **2012**, *24*, 1067.
[11] Y. J. Kim, S.-E. Chun, J. Whitacre, C. J. Bettinger, *J. Mater. Chem. B* **2013**, *1*, 3781.
[12] M. L. Hammock, A. Chortos, B. C.-K. Tee, J. B. -H. Tok, Z. Bao, *Adv. Mater.* **2013**, *25*, 5997.

[13] S. Bauer, S. Bauer-Gogonea, I. Graz, M. Kaltenbrunner, C. Keplinger, R. Schwödiauer, *Adv. Mater.* **2014**, *26*, 149.
[14] S.-W. Hwang, G. Park, H. Cheng, J.-K. Song, S.-K. Kang, L. Yin, J.-H. Kim, F. G. Omenetto, Y. Huang, K.-M. Lee, J. A. Rogers, *Adv. Mater.* **2014**, *26*, 3905.
[15] M. Kaltenbrunner, M. S. White, E. D. Głowacki, T. Sekitani, T. Someya, N. S. Sariciftci, S. Bauer, *Nat. Commun.* **2012**, *3*, 770.
[16] M. S. White, M. Kaltenbrunner, E. D. Głowacki, K. Gutnichenko, G. Kettlgruber, I. Graz, S. Aazou, C. Ulbricht, D. A. M. Egbe, M. C. Miron, Z. Major, M. C. Scharber, T. Sekitani, T. Someya, S. Bauer, N. S. Sariciftci, *Nat. Photonics* **2013**, *7*, 811.
[17] M. Kaltenbrunner, T. Sekitani, J. Reeder, T. Yokota, K. Kuribara, T. Tokuhara, M. Drack, R. Schwödiauer, I. Graz, S. Bauer-Gogonea, S. Bauer, T. Someya, *Nature* **2013**, *499*, 458.
[18] R. C. Webb, A. P. Bonifas, A. Behnaz, Y. Zhang, K. J. Yu, H. Cheng, M. Shi, Z. Bian, Z. Liu, Y.-S. Kim, W.-H. Yeo, J. S. Park, J. Song, Y. Li, Y. Huang, A. M. Gorbach, J. A. Rogers, *Nat. Mater.* **2013**, *12*, 938.
[19] M. Jablonski, F. Bossuyt, J. Vanfleteren, T. Vervust, H. de Vries, *Microelectron. Reliab.* **2013**, *53*, 956.
[20] S. P. Lacour, J. Jones, S. Wagner, T. Li, Z. Suo, *Proc. IEEE* **2005**, *93*, 1459.
[21] S. Wagner, S. Bauer, *MRS Bull.* **2012**, *37*, 207.
[22] J. Ho, T. R. Jow, S. Boggs, *IEEE Electrical Insulation Mag.* **2010**, *26*, 20.
[23] L. Qi, L. Petersson, T. Liu, *J. Int. Council Electrical Eng.* **2014**, *4*, 1.
[24] S. Rosset, H. R. Shea, *Appl. Phys. A* **2013**, *110*, 281.
[25] I. M. Graz, D. P. J. Cotton, S. P. Lacour, *Appl. Phys. Lett.* **2009**, *94*, 071902.
[26] A. P. Robinson, I. Minev, I. M. Graz, S. P. Lacour, *Langmuir* **2011**, *27*, 4279.
[27] D. Brosteaux, F. Axisa, M. Gonzalez, J. Vanfleteren, *IEEE Electron. Dev. Lett.* **2007**, *28*, 552.
[28] Y. Zhang, S. Xu, H. Fu, J. Lee, J. Su, K.-C. Hwang, J. A. Rogers, Y. Huang, *Soft Matter* **2013**, *9*, 8062.
[29] D.-Y. Khang, H. Jiang, Y. Huang, J. A. Rogers, *Science* **2006**, *311*, 208.
[30] T. Sekitani, Y. Noguchi, K. Hata, T. Fukushima,T. Aida , T. Someya, *Science* **2008**, *321*, 1468.
[31] M. Park, J. Park, U. Jeong, *Nano Today* **2014**, *9*, 244.
[32] J. Liang, L. Li, K. Tong, Z. Ren, W. Hu, X. Niu, Y. Chen, Q. Pei, *ACS Nano* **2014**, *8*, 1590.
[33] M.-S. Lee, K. Lee, S.-Y. Kim, H. Lee, J. Park, K.-H. Choi, H.-K. Kim, D.-G. Kim, D.-Y. Lee, S. W. Nam, J.-U. Park, *Nano Lett.* **2013**, *13*, 2814.
[34] D. J. Lipomi, M. Vosgueritchian, B. C. Tee, S. L. Hellstrom, J. A. Lee, C. H. Fox, Z. Bao, *Nat. Nanotechnol.* **2011**, *6*, 788.
[35] J. Zang, S. Ryu, N. Pugno, Q. Wang, Q. Tu, M. J. Buehler, X. Zhao, *Nat. Mater.* **2013**, *12*, 321.
[36] C. Keplinger, J.-Y. Sun, C. C. Foo, P. Rothemund, G. M. Whitesides, Z. Suo, *Science* **2013**, *341*, 984.
[37] J. A. Rogers, *MRS Bull* **2014**, *39*, 514.
[38] J. Zang, X. Zhao, Y. Cao, J. W. Hutchinson, *J. Mech. Phys. Solids* **2012**, *60*, 1265.
[39] I. M. Graz, D. P. J. Cotton, A. Robinson, S. P. Lacour, *Appl. Phys. Lett.* **2011**, *98*, 124101.
[40] A. Robinson, A. Aziz, Q. Liu, Z. Suo, S. P. Lacour, *J. Appl. Phys.* **2014**, *115*, 143511.
[41] F. Axisa, D. Brosteaux, E. De Leersnyder, F. Bossuyt, J. Vanfleteren, B. Hermans, R. Puers, 29th Annual Int. Conf. Engineering in Medicine and Biology Society (EMBS), IEEE, **2007**, p. 5687, DOI: 10.1109/IEMBS.2007.4353637.
[42] S. Xu, Y. Zhang, L. Jia, K. E. Mathewson, K.-I. Jang, J. Kim, H. Fu, X. Huang, P. Chava, R. Wang, S. Bhole, L. Wang, Y. J. Na, Y. Guan, M. Flavin, Z. Han, Y. Huang, J. A. Rogers, *Science* **2014**, *344*, 70.
[43] H. Cheng, Y. Zhang, K-C Hwang, J. A. Rogers, Y. Huang, *Int. J. Solids Struct.* **2014**, *51*, 3113.
[44] D. J. Lipomi, J. A. Lee, M. Vosgueritchian, B. C.-K. Tee, J. A. Bolander, Z. Bao, *Chem. Mater.* **2012**, *24*, 373.